Catalysis Science & Technology

www.rsc.org/catalysis

Volume 3 | Number 10 | October 2013 | Pages 2447–2850

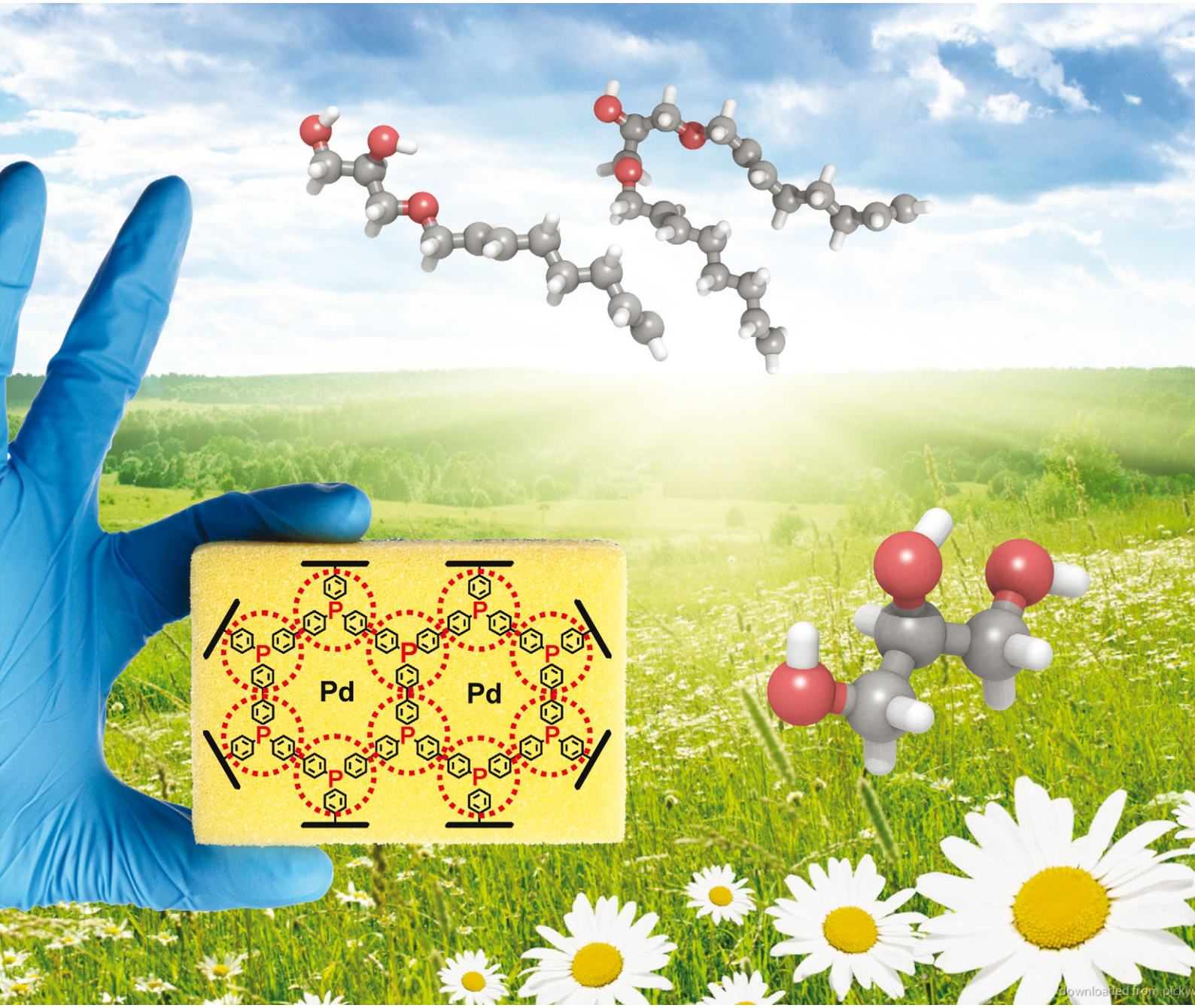

ISSN 2044-4753

RSC Publishing

COVER ARTICLE

Klein Gebbink, Bruijnincx *et al.*

Development of a 4,4′-biphenyl/phosphine-based COF for the heterogeneous Pd-catalysed telomerisation of 1,3-butadiene

2044-4753(2013)3:10;1-6

Catalysis
Science & Technology

RSC Publishing

PAPER

View Article Online
View Journal | View Issue

Cite this: *Catal. Sci. Technol.*, 2013, **3**, 2571

Development of a 4,4′-biphenyl/phosphine-based COF for the heterogeneous Pd-catalysed telomerisation of 1,3-butadiene†

Peter J. C. Hausoul,[ab] Tamara M. Eggenhuisen,[a] Deepak Nand,[c] Marc Baldus,[c] Bert M. Weckhuysen,[a] Robertus J. M. Klein Gebbink*[b] and Pieter C. A. Bruijnincx*[a]

Received 21st March 2013,
Accepted 2nd July 2013

DOI: 10.1039/c3cy00188a

www.rsc.org/catalysis

The improved synthesis, characterisation and application of a microporous 4,4′-biphenyl/phosphine-based covalent organic framework (COF) for the heterogeneous Pd-catalysed telomerisation of 1,3-butadiene with phenol and glycerol are presented. The solid polyphosphine is amorphous, microporous and an excellent support for $Pd(acac)_2$. Solid-state NMR and DRIFT analysis of materials of varying Pd-loading show that bis-phosphine complexes of palladium are preferably formed. Under solvent- and base-free conditions, high conversions and selectivities are obtained for this catalyst material with both phenol and glycerol as substrates. The product selectivity, with both butenylation and telomerisation activity observed with phenol, can be tuned by variation of the metal loading. For glycerol it is shown that the selectivity to the undesired tri telomer is low under all applied conditions and, remarkably, that the heterogeneous catalyst outperforms its homogeneous PPh_3-based counterpart.

Introduction

The development of catalyst materials that combine the advantages of both homogeneous and heterogeneous catalysis is a major challenge in chemistry. For this purpose, many different approaches have been explored. Well-known examples include the immobilisation of transition metal complexes on (in)organic supports (*e.g.*, *via* covalent or ionic attachment to polymers and dendrimers or silicas, zeolites and clays) or the deposition/encapsulation of small metal particles in porous solid matrices (*e.g.* polymers or zeolites).[1,2] Currently, attention is shifting towards the development of functional materials, such as metal organic frameworks (MOFs), covalent organic frameworks (COFs) and porous organic polymers (POPs). In particular for those reactions that are catalysed by metal complexes, the construction of polymeric materials from rigid, ligand-containing units offers several advantages over the more traditional approach of attaching ligands to preformed materials by post-synthetic modification methods. These new functional polymers often possess larger surface areas, show improved site isolation, prevent ligand loss and allow direct immobilisation of metal species on the (polymer) backbone. In this way, more control can be exerted over the catalyst environment as well as on relevant parameters such as the ligand to metal ratio and metal loading.[3,4] Recent examples of this approach include a Ca/tris(*p*-carboxylatophenyl)-phosphine based MOF studied for gas absorption and separation applications,[5] a triazine-based COF applied for the Pt-catalysed oxidation of methane to methanol,[6] and an imine-based COF[7] and 4,4′-biphenyl/phosphonium-based POP, both of which were used in the Pd-catalysed Suzuki coupling.[8]

The telomerisation of 1,3-butadiene is a versatile and commercially applied method for the functionalisation of a broad range of (multifunctional) nucleophiles (Scheme 1, ROH = MeOH, diols, glycerol, carbohydrates, *etc.*).[9] Homogeneous Pd/PR_3[10,11] or Pd/NHC[12] (NHC: N-heterocyclic carbene) catalysts are typically used for, for instance, methanol telomerisation owing to their high activity and chemoselectivity towards the desired linear (n) telomer. In this particular case, the volatility of the methanol telomers ensures that product isolation and catalyst recovery are easily achieved. For the Pd/PR_3-catalysed telomerisation with biomass-based alcohols, the telomer products are generally non-volatile, however, and recovery of the catalyst remains a serious issue. The development of a facile synthesis of a robust heterogeneous phosphine-based catalyst is therefore highly desired, also given the broader applicability of such a material in other metal/phosphine-catalysed reactions.

[a] *Inorganic Chemistry & Catalysis, Debye Institute for Nanomaterials Science, Utrecht University, Universiteitsweg 99, 3584 CG, Utrecht, The Netherlands. E-mail: p.c.a.bruijnincx@uu.nl; Fax: +31 30 251 1027; Tel: +31 30 253 7400*
[b] *Organic Chemistry & Catalysis, Debye Institute for Nanomaterials Science, Utrecht University, Universiteitsweg 99, 3584 CG, Utrecht, The Netherlands. E-mail: r.j.m.kleingebbink@uu.nl; Fax: +31 30 252 3615; Tel: +31 30 253 3120*
[c] *NMR Spectroscopy Research Group, Bijvoet Center for Biomolecular Research, Utrecht University, Padualaan 8, 3584 CH, Utrecht, The Netherlands*

† Electronic supplementary information (ESI) available. See DOI: 10.1039/c3cy00188a

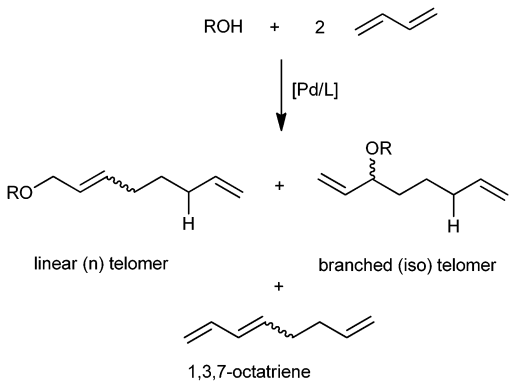

Scheme 1 Overall reaction of the Pd/L-catalysed telomerisation of 1,3-butadiene with alcohols (ROH).

Several heterogeneous catalyst systems have been developed for telomerisation reactions. Relevant examples include resin bound Pd–phosphine complexes,[13] Pd particles on inorganic supports (*e.g.*, Pd/Al_2O_3),[14] or, as an alternative approach to the catalyst separation issue, a Pd/TPPTS-based (TPPTS: 3,3′,3″-phosphinidyne-tris(benzenesulfonic acid) trisodium salt) aqueous biphasic system.[9,15] These studies typically showed that the use of additional bases as co-catalysts (*e.g.*, NaOR, NR_3 and KF) led to improved catalyst activity. Recently, we have reported a LDH/Pd/TPPTS-based (LDH: layered double hydroxide) catalyst for the telomerisation of methanol and ethylene glycol, a system in which the base is incorporated into the catalyst support.[16] Ion exchange of TPPTS onto the basic inorganic support resulted in an active telomerisation system. Interestingly, product selectivity changed from C8 telomers to telomers with longer carbon chains (carrying C16 fragments in particular). These products were proposed to originate from C–C coupling reactions between mobile reactive intermediates thought to exist in high local concentrations on the support. To further advance the development of heterogeneous telomerisation catalysts, we set out to prepare a phosphine-based COF designed to prevent selectivity issues that result from such phosphine mobility by improving site isolation, as well as to provide a Lewis basic and recoverable support with high loading capacity for molecular palladium complexes.

Recent reports by Kaskel *et al.* detail the preparation of COFs with high porosities and surface areas in which heteroatoms, initially Si, Sn, and Bi and most recently also P, are cross-linked with 4,4′-biphenyl spacers.[17] Catalytic studies on these materials demonstrated that the incorporated heteroatoms behave comparably to their homogeneous counterparts and that the phosphorus-based materials allow immobilization of transition metal complexes (*e.g.*, $PdCl_2$, $RuCl(PPh_3)_3$) *via* simple impregnation methods. However, as in the case of the 4,4′-biphenyl/phosphonium COF,[8] characterisation of the material by ^{31}P NMR revealed that a considerable portion of the incorporated phosphorus atoms are either oxidized or quarternarized. Therefore, the development of a synthesis procedure for such P-based COFs that leads to a material that is more pure in terms of phosphorus species is of great interest. Furthermore, the coordination behaviour of the material as well as the nature of the metal complexes formed is still poorly understood. Here, we present an alternative synthesis procedure, developed in parallel to the work of Kaskel and co-workers, for the 4,4′-biphenyl/phosphine COF **1**, leading to high PAr_3 content and a detailed study of the coordination chemistry of this solid P-ligand with $Pd(acac)_2$. Furthermore, the application of this material as a catalyst support in the solvent and base-free Pd-catalysed telomerisation of 1,3-butadiene with phenol and glycerol is presented.

Results and discussion

Synthesis and characterization

The 4,4′-biphenyl/phosphine COF **1** was prepared in a one-pot process starting with the dilithiation of 4,4′-dibromobiphenyl with excess ^nBuLi in Et_2O at room temperature (RT) for 1 h. During reaction, the dilithio compound precipitated out of solution and was subsequently filtered and washed with Et_2O and hexane to remove the ^nBuBr formed as well as excess ^nBuLi.[18] The purified dilithio compound was subsequently suspended in THF and a solution of PCl_3 in THF was slowly added at RT over 3 h. To the dark purple precipitate formed in this procedure, an excess of PhLi was added to the reaction to convert any remaining $PArCl_2$ or PAr_2Cl groups in the material, ensuring that all phosphines are of the PAr_3 type (Scheme 2). After overnight stirring, the reaction was quenched with MeOH. The resulting material was washed repeatedly and finally dried overnight *in vacuo* at 60 °C. A fluffy, pale yellow polymer (**1**) insoluble in common organic solvents was obtained. Loss of the polymer during washing and filtration was found to be negligible. SEM images of **1** show that the material consists of particles that are typically larger than 1 μm, but have a very broad particle size distribution. The larger particles in turn appear to be composed of aggregated smaller particles that are typically larger than 60 nm (Fig. 1).

The XRD pattern of **1** (see Fig. S2, ESI†) shows very broad and weak peaks at 20°, 35° and 50° 2θ, suggesting that the structure is generally amorphous, but does exhibit some local ordering.

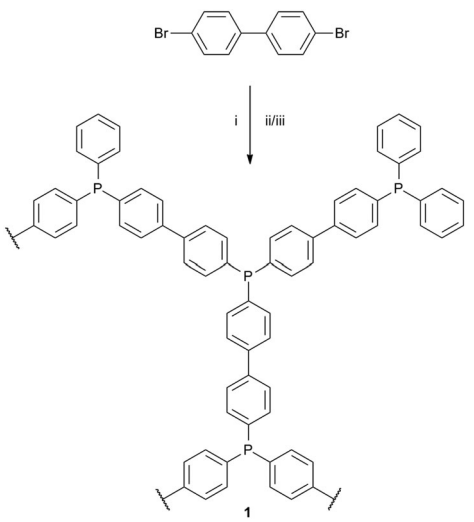

Scheme 2 Synthesis and structure of **1**. Conditions: (i) Et_2O, 4 eq. ^nBuLi, RT, 1 h; (ii) THF, 2/3 eq. PCl_3, RT, 3 h; (iii) THF, 1 eq. PhLi, RT, 18 h.

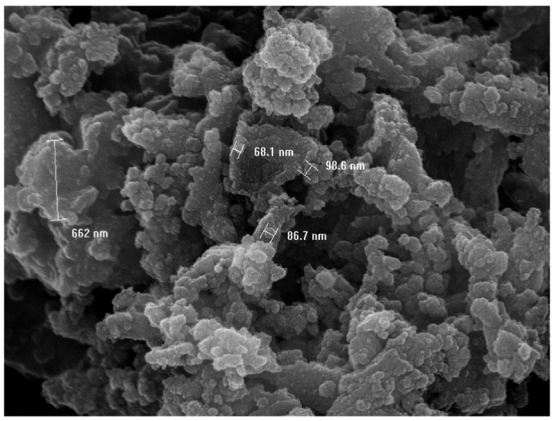

Fig. 1 SEM image of **1** showing the aggregation of smaller particles.

No phase transitions could be detected by DSC (Fig. S4, ESI†) between −50 and 200 °C. TGA showed some weight loss (4.4%, possibly due to solvent evaporation) between 25 to 150 °C, while decomposition of **1** occurs only at 380 °C (Fig. S3, ESI†). The BET surface area, determined by N_2 physisorption, is 135 $m^2\ g^{-1}$ (Fig. S5, ESI,† pore volume of 0.04 $cm^3\ g^{-1}$). These results suggest that the structure of the polymeric material is largely unordered[19] and that the material is microporous. However, compared to the phosphonium (BET area: 650–980 $m^2\ g^{-1}$)[8] and phosphine (BET area: 458–646 $m^2\ g^{-1}$)[17] analogues reported before, **1** exhibits a considerably lower surface area and pore volume. This is likely the result of a filling of the pores by the reaction of PhLi with defect sites within the material. The chemical composition of the polymer backbone of **1** was assessed using ^{13}C and ^{31}P solid-state NMR under magic-angle spinning (MAS, see, *e.g.*, ref. 20) conditions. The ^{31}P NMR spectrum displays an intense, broad peak at −4.9 ppm, assigned to the phosphine of **1**, and a very weak peak at 34.3, which is likely the phosphine oxide (Fig. 2, top).

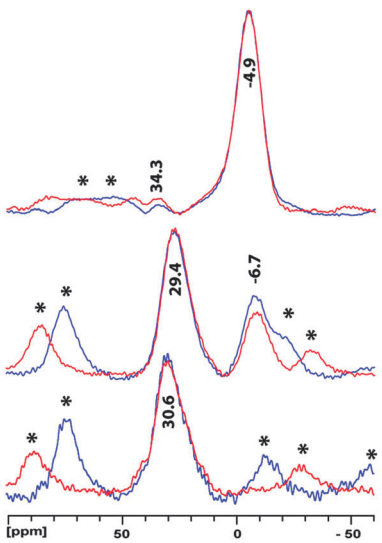

Fig. 2 Solid-state MAS ^{31}P NMR spectra of **1** (top), 0.33Pd@**1** (middle) and 0.52Pd@**1** (bottom). 1D spectra were recorded with MAS rates of 10 kHz (blue) and 12 kHz (red) to identify spinning side bands (*).

The ^{31}P chemical shift of **1** is observed slightly downfield as compared to the closest model compounds PPh_3 and tri([1,1′-biphenyl]-4-yl)phosphine, which resonate at −5.8 and −12.4 ppm in solution, respectively.[21,22] The ^{13}C NMR spectrum of **1** (Fig. S6, ESI†) only shows three strongly overlapping signals at 142, 135 and 129 ppm, which are assigned to the aromatic rings in **1**. These data confirm that the synthesis method yields a polymer in which all phosphorus atoms are substituted with either biphenyl or phenyl groups.

Coordination studies

The coordination behaviour of **1** towards Pd(0) and Pd(II) was studied using $Pd(dba)_2$ (dba: dibenzylideneacetone) and $Pd(acac)_2$ (acac: acetylacetonato). Stirring **1** with $Pd(dba)_2$ in toluene resulted in the formation of a black solid, indicating the decomposition of the Pd(0) complex and aggregation to palladium black particles. In contrast, stirring **1** with 1.2 eq. of $Pd(acac)_2$ (w.r.t. to the molar amount of phosphorus in the polymer) in methanol resulted in an orange solid. TEM analysis showed no palladium particles on the material. After centrifugation, decantation and drying *in vacuo*, a ligand to metal ratio (P/Pd) of 1.9 was found as determined by elemental analysis. For this Pd-loaded material (0.52Pd@**1**), TGA measurements showed weight loss steps at 120 °C and 380 °C, corresponding to the successive decomposition of the supported Pd species and the support (Fig. S7, ESI†). As a result of metal incorporation, the BET surface area and pore volume are further reduced to 58 $m^2\ g^{-1}$ and 0.009 $cm^3\ g^{-1}$, respectively (Fig. S8, ESI†).

The ^{31}P NMR spectrum of 0.52Pd@**1** showed just a single broad peak at 30.6 ppm, with the peak for the free phosphine being completely absent (Fig. 2, bottom). Thus despite the rather low surface area and porosity of **1**, these data suggest that all phosphine sites in the material are accessible for coordination and are affected by only 0.52 eq. of $Pd(acac)_2$. This is rather remarkable as it implies that mainly bisphosphine ligated Pd sites are formed (Scheme 3). A material with a P/Pd ratio of 3.0 (0.33Pd@**1**) was also prepared and its ^{31}P NMR spectrum showed two separate peaks at 29.4 and −6.7 ppm, with an approximate integral ratio of 2 : 1 (Fig. 2, middle). This result rules out the

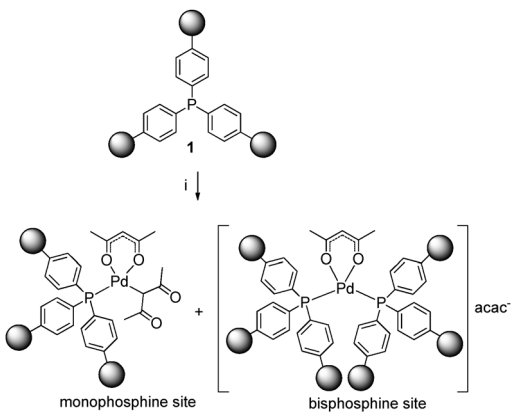

Scheme 3 Proposed metal species formed upon loading of **1** with $Pd(acac)_2$. Conditions: (i) $Pd(acac)_2$, MeOH, RT, overnight.

possibility of dynamic behaviour within the material and further confirms the propensity towards bisphosphine ligation in **1**. The solution ^{31}P chemical shifts of reference compounds [Pd(acac)$_2$(PPh$_3$)] (31 ppm) and [Pd(acac)(PPh$_3$)$_2$]BF$_4$ (36 ppm) are both close to the chemical shift found for 0.52Pd@**1** and 0.33Pd@**1**. As a result of the severe broadening of the signal, it is unclear, however, if the peak of 0.52Pd@**1** is composed of one or multiple peaks. The ^{13}C NMR spectra of 0.52Pd@**1** (see Fig. S9, ESI†) and 0.33Pd@**1** showed, next to the signals of **1**, three additional signals at 188.9, 102.2 and 28.4 ppm, which are assigned to *O*,*O*-bonded acac ligands. Interestingly, signals corresponding to *C*-bonded acac ligands were not observed. The DRIFT spectrum of 0.52Pd@**1** showed absorption bands at 1577 cm^{-1} and 1675 cm^{-1}, which are reported to correspond to the CO stretch of the carbonyl groups of *O*,*O*-bonded and *C*-bonded acac ligands, respectively (Fig. 3).[23] *C*-bonded acac ligands are typically observed for Pd(acac)$_2$(PR$_3$) complexes with only one phosphine ligand (Scheme 3). This bonding mode is nonetheless not confirmed by ^{13}C NMR, which only shows signals for *O*,*O*-bonded acac ligands. Indeed, it is known that in solution the presence of excess phosphine leads to decoordination of one acac ligand and the formation of stable *cis*-[Pd(acac)(PR$_3$)$_2$]$^+$ complexes.[24] In keeping with these results, we propose that the vibrations between 1625–1675 cm^{-1} correspond to non-ligated acac anions.

Additional materials with P/Pd ratios of 6.5 (0.16Pd@**1**), 3.5 (0.29Pd@**1**), and 0.9 (1.07Pd@**1**) were prepared by stirring **1** and Pd(acac)$_2$ in methanol, and subsequently concentrating the solution *in vacuo* without filtration. The DRIFT spectra of these materials (Fig. 3) all show peaks for both *O*,*O*-bonded and displaced acac ligands. The rather broad peak shape of the CO stretch between 1625–1675 cm^{-1} (*i.e.*, for 0.16Pd@**1** and 0.29Pd@**1**) indeed suggests that the environment of the displaced acac is much less defined than that of the *O*,*O*-bonded acac observed at 1577 cm^{-1}. Interestingly, the absorbance of the displaced acac does not increase going from 0.52Pd@**1** to 1.07Pd@**1**, while the signals corresponding to *O*,*O*-bonded acac do become more intense. TEM analysis shows that this can be explained by the formation of small crystallites of 0.3–1 nm with 1.07Pd@**1**, nanoparticles that are homogeneously distributed throughout the material (Fig. S10, ESI†). In line with the ^{31}P NMR data, this suggests that at a P/Pd ratio of 2 all available coordination sites are occupied and any excess Pd(acac)$_2$ is deposited on or in the material during drying. Overall, the data above provide evidence that phosphine material **1** has the strong tendency to create bis(phosphine)-ligated Pd centres, although the formation of mono(phosphine)-ligated Pd centres cannot be fully excluded. It appears therefore that the average distance between adjacent phosphorus centres in **1** is sufficiently small to allow chelate binding. The XRD spectrum of **1** shows that some local ordering exists in the materials. The peaks shapes and positions are reminiscent of amorphous carbon and suggest the presence of π–π stacking interactions. For **1**, optimal π–π stacking interactions are achieved when the biaryl spacers are aligned. As such, the phosphorus centers are placed in close proximity to each other. Furthermore, although stable *cis* (P–Pd–P = 90°) and *trans* (P–Pd–P = 180°) geometries are typically observed for molecular complexes, depending on the constraints imposed by the ligand, significant deviations from these optimal geometries are also found to be stable. Although in the case of **1** the phosphine centres are, more or less, fixed in space as a result of the cross-linked polymeric structure, the random growth and amorphous nature of the polymer may allow some contraction or reorganisation to occur upon metal binding and drying, consequently improving the stability of chelate binding.

Telomerisation of 1,3-butadiene with phenol

The catalytic activity of the Pd-loaded materials was initially tested in the telomerisation of 1,3-butadiene with phenol (**2**) (Scheme 4). Reactions were performed at 80 °C for 1 h with a butadiene to substrate ratio (Bu/**2**) of 2 and a metal loading of 0.16 mol% with respect to **2**. It is important to note that these reactions were run under neat conditions, *i.e.*, no additional solvent was used, and without the use of any added base. In these reactions linear and branched butenyl C4 products (**2a** and **2b**) were also formed in addition to the expected linear and branched C8 telomers (**2c** and **2d**) (Table 1). Interestingly, the selectivity of the catalyst strongly depended on the

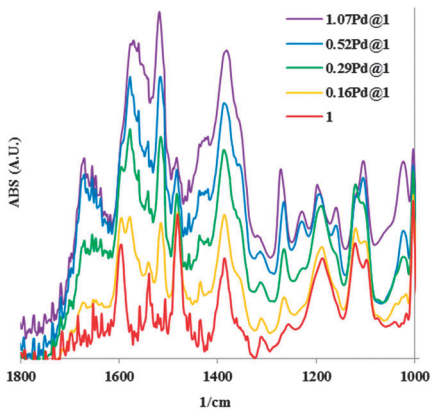

Fig. 3 Overlay of DRIFT spectra of **1** and the Pd(acac)$_2$-loaded materials 0.16Pd@**1**, 0.29Pd@**1**, 0.52Pd@**1** and 1.07Pd@**1**.

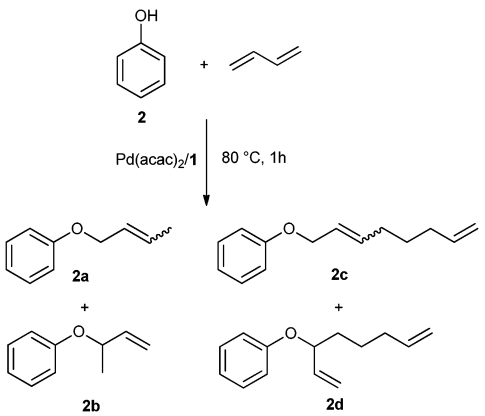

Scheme 4 Pd(acac)$_2$/**1**-catalysed telomerisation of 1,3-butadiene with phenol (**2**).

Table 1 Influence of the P/Pd ratio on the $Pd(acac)_2$/**1**-catalysed telomerisation of butadiene with **2**

Entry	P/Pd	Bu/**2**	Conv. **2** (%)	Sel. C4 (%)	Sel. C8 (%)	n/iso C4 **2a**/**2b**	n/iso C8 **2c**/**2d**
1	0.8	2.2	98	1	99	0.4	7.3
2	1.6	2.2	99	2	98	0.6	3.8
3	3.0	2.4	100	8	92	1.8	3.3
4	6.6	2.1	100	14	86	1.8	3.7
5	12.9	2.1	60	67	33	1.2	10.2

Conditions: 0.16–0.17 mol% $Pd(acac)_2$, 80 °C, 1 h.

P/Pd ratio. At low P/Pd ratios, the reaction reached (near) full conversion and high C8 selectivities of between 92 and 99% were obtained. At higher P/Pd ratios, the C4 selectivity increased to 67% and the conversion of **2** decreased to 60%, indicating a drop in telomerisation activity. The linear to branched ratios (n/iso) of the C4 products were low (*i.e.*, 0.4–1.8) in all cases, whereas the C8 n/iso ratio varied with the P/Pd ratio.

Catalytic and mechanistic studies on the homogeneous Pd-catalysed telomerisation reaction have shown that etherification *via* monophosphine complexes generally results in n/iso ratios larger than 10. The participation of bisphosphine complexes, which result from excess phosphine in the reaction mixture, leads to a drastic drop in chemoselectivity.[25] In addition, a study by Goux *et al.* on the etherification of phenols *via* *cis*-$[Pd(\pi\text{-allyl})(PR_3)_2]^+$ complexes showed that the reaction may proceed under kinetic or thermodynamic control depending on the reaction temperature.[26] Under kinetic conditions n/iso ratios between 0.6 and 1.6 were found, whereas under reversible conditions the n/iso ratio increased to 2.5. It should also be noted that Jolly *et al.* and Kuntz *et al.* have previously shown that the Pd-catalysed butenylation reaction of MeOH and H_2O (*i.e.*, 1 : 1 adduct formation), which solely involves bisphosphine complexes as catalytic intermediates, proceeds separately from telomerisation.[27] The Pd/**1**-catalysed formation of both butenyl and octadienyl ethers therefore indicates that **1** possesses both monophosphine and bisphosphine sites under working conditions, sites which catalyse telomerisation and butenylation reactions, respectively. As discussed above, the IR and NMR data of the dried catalyst materials, clearly point to the formation of bis-ligated Pd centres. However, under catalytic conditions, elevated temperature, solvation and enhanced ligand exchange each contribute to the conversion of bisphosphine sites to monophosphine sites. Also, due to the microporous nature of the polymer and the resulting diffusion limitation, it is likely that catalysis occurs primarily at the surface layer of the material, which necessarily contains a higher proportion of monophosphine sites. Nevertheless, as a result of the higher binding affinity of bisphosphine sites, such sites will be preferably occupied first. This is indeed reflected in the results shown in entry 5 of Table 1, where, as a result of the high P/Pd ratio, the C4 selectivity exceeds that of the C8 selectivity. The lower phenol conversion in this case also suggests that butenylation is a reaction that is slower than telomerisation. The relatively low n/iso ratios of the C8 products indicate that equilibration of the product composition may also be a factor influencing the n/iso ratio.[25b,26]

Table 2 Influence of metal-loading on the $Pd(acac)_2$/**1**-catalysed telomerisation of butadiene with **2**

Entry	[Pd] (mol%)	Bu/**2**	Conv. **2** (%)	Sel. C4 (%)	Sel. C8 (%)	n/iso C4 **2a**/**2b**	n/iso C8 **2c**/**2d**
1	0.16	2.2	99	2	98	0.6	3.8
2	0.05	2.6	100	2	98	0.4	10.1
3	0.05	4.3	100	2	98	0.3	15.3
4	0.02	2.2	43	3	97	0.4	14.8

Conditions: P/Pd = 1.6, 80 °C, 1 h.

The influence of the catalyst loading on product composition was studied using a catalyst with a fixed P/Pd ratio of 1.6. Table 2 shows that lowering the catalyst loading resulted in a marked increase of the n/iso ratio of C8 products to 14.8 and a lowering of the n/iso ratio of the C4 products to 0.4, whereas C4 and C8 selectivities were not affected. Increasing the Bu/**2** ratio to 4 resulted in a similar effect. These results show that at lower loadings or higher dilutions, the reaction proceeds under kinetic control and that equilibration of the n/iso ratio is much slower.

Telomerisation of 1,3-butadiene with glycerol

Next, the activity of **1** was tested in the biphasic telomerisation of butadiene with glycerol (**3**) (Scheme 5). Also for **3**, reactions were run neat and without any added base. The reaction yields a mixture of linear and branched isomers of mono (**3a**), di (**3b**) and tri (**3c**) telomers, but C4 products or higher telomers were not detected. After 16 h at 80 °C, the introduced butadiene was fully consumed and good glycerol conversions (55–84%) and high selectivities towards **3a** (41–52%) and **3b** (41–53%) were observed (Table 3). The formation of **3c**, in contrast, remained below 8% in all cases. Notably, the mono and di telomer selectivities are not influenced by the P/Pd ratio, whereas the n/iso ratios, which are higher for the mono telomers, significantly increased with the P/Pd ratio. TEM analysis of the spent catalysts recovered by filtration revealed that Pd particles of various sizes (1–10 nm) were deposited on the exterior of the catalyst (*i.e.*, particles were found primarily on the edges, Fig. 4). In particular the spent catalysts of high initial Pd loading (low P/Pd ratio) contained large clusters of Pd particles.

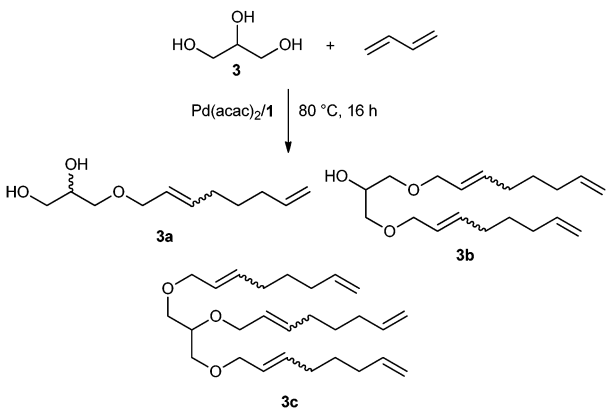

Scheme 5 $Pd(acac)_2$/**1**-catalysed telomerisation of 1,3-butadiene with glycerol (**3**) (branched products and isomers not shown for clarity).

Table 3 Influence of the P/Pd ratio on the $Pd(acac)_2$/**1**-catalysed telomerisation of butadiene with **3**

Entry	P/Pd	Bu/**3**	Conv. **3** (%)	Sel. **3a** (%)	Sel. **3b** (%)	Sel. **3c** (%)	n/iso **3a**	n/iso **3b**
1	0.9	3.1	61	51	41	8	8.8	4.1
2	1.9	2.6	55	41	53	6	9.3	5.9
3	3.5	2.9	71	43	52	5	10.7	7.0
4	6.5	3.5	84	52	46	3	15.7	7.5

Conditions: 0.10–0.12 mol% $Pd(acac)_2$, 80 °C, 16 h.

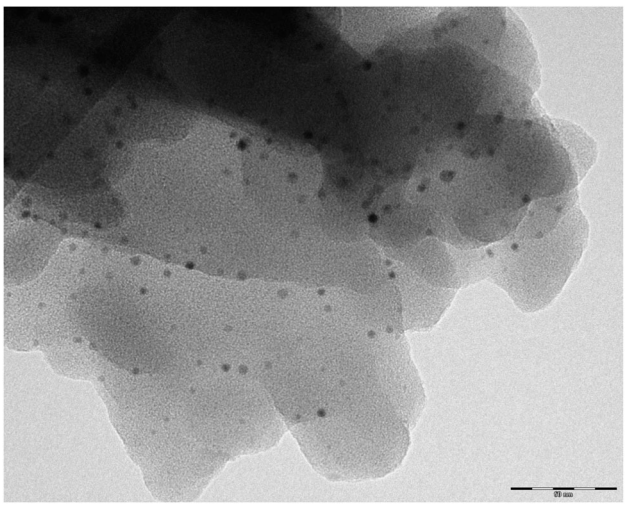

Fig. 4 TEM image of a spent catalyst used in the telomerization of **3** (P/Pd = 1.9, Table 3, entry 2), showing the presence of small Pd particles.

Table 4 lists the composition of fresh and spent catalysts and residual Pd in the product phase. The results show that at low initial P/Pd ratios (entries 1 and 2) considerable leaching (36–48%) occurred. In contrast, a high initial P/Pd ratio (entries 3 and 4) significantly reduced leaching of the metal (7–13%). Combined with the corresponding catalytic results, these data clearly show that increasing the P/Pd ratio reduces metal leaching without compromising catalytic activity, while concomitantly improving product selectivity. The P/Pd ratio therefore offers an effective handle to optimize the performance of the catalyst and reduce metal leaching.

Furthermore, owing to the high affinity of **1** for Pd(0) the facile recapture of metal particles formed in solution provides an additional mechanism for limiting metal loss and contamination of the telomer product. It is therefore expected that **1** can also be employed as a ''sponge'' for recovering precious transition metals from catalytic mixtures.

Table 4 P/Pd ratios of fresh and spent catalysts and Pd-leaching in the telomerisation of butadiene with **3** (entries correspond to catalytic data reported in Table 3)

Entry	Fresh P/Pd[a]	Spent P/Pd[a]	[Pd] solution[b] (ppm)	Pd loss (%)
1	0.9	—	67.5	48
2	1.9	2.7	50.5	36
3	3.5	3.8	18.5	13
4	6.5	7.2	9	7

[a] Determined by EA. [b] Determined by ICP.

Table 5 Influence of the Bu/**3** ratio on the $Pd(acac)_2$/**1**-catalysed telomerisation of butadiene with **3**

Entry	Bu/**3**	Conv. **3** (%)	Sel. **3a** (%)	Sel. **3b** (%)	Sel. **3c** (%)	n/iso **3a**	n/iso **3b**
1	1.8	46	45	50	5	9.6	6.1
2	3.3	81	56	40	4	16.4	9.1
3	6.3	99	32	63	5	9.7	5.7

Conditions: 0.10–0.12 mol% $Pd(acac)_2$, P/Pd = 3.5, 80 °C, 16 h.

Table 6 Influence of the P/Pd ratio on the $Pd(acac)_2$/**1**-catalysed telomerisation of butadiene with **3**

Entry	[Pd] (mol%)	Bu/**3**	Conv. **3** (%)	Sel. **3a** (%)	Sel. **3b** (%)	Sel. **3c** (%)	n/iso (**3a**)	n/iso (**3b**)
1	0.115	1.8	46	45	50	5	9.6	4.1
2	0.053	1.9	49	46	50	4	13.4	5.9
3	0.026	2.1	49	41	55	4	11.0	7.0
4[a]	0.056	2.0	<1	—	—	—	—	—

Conditions: P/Pd = 3.5, 80 °C, 16 h. [a] Reaction with PPh_3, P/Pd = 4.1.

Variation of the Bu/**3** ratio was studied using a catalyst with a P/Pd ratio of 3.5 and the results show that the conversion of glycerol increased with increasing Bu/**3** ratio (Table 5). Interestingly, the formation of **3c** remains constant and low, whereas the selectivity of **3b** increases at the expense of **3a** at full glycerol conversion. The influence of the metal loading was studied using a catalyst with P/Pd of 3.5 and a Bu/**3** ratio of 2 (Table 5, entries 1–3). Full butadiene consumption was observed for each of these reactions, indicating that the reactions are completed within 16 h. Lowering the catalyst loading (*i.e.*, while keeping the P/Pd ratio constant) from 0.115 to 0.026 mol% did not noticeably affect the product distribution, whereas the TON considerably increased from 571 to 2976 (Table 6).

Since the butadiene conversion is complete in these reactions, these data show that significant room for improvement of the TON still remains. In contrast to phenol telomerisation experiments (Table 2), it appears that for glycerol telomerisation equilibration of the n/iso ratio does not occur to a noticeable degree. Surprisingly, a benchmark reaction run with PPh_3 as homogeneous ligand and with the same P/Pd ratio as well as metal loading gave only negligible conversion (Table 6, entry 4). This clearly demonstrates that **1** is superior to PPh_3 for glycerol telomerisation as, contrary to typical heterogenized catalysts, it outperforms its homogeneous counterpart.

Conclusions

An improved synthesis of the 4,4′-biphenyl/phosphine-based COF (**1**) is presented, resulting in a well-defined framework with high PAr_3 content. Characterisation and coordination studies show that the polymeric material is amorphous, microporous and an excellent support for $Pd(acac)_2$. Solid-state NMR

and DRIFT data of Pd-loaded materials provide evidence that all coordination sites are accessible and that the incorporated metal species mainly form bisphosphine complexes. The results of the heterogeneously catalysed telomerisation of butadiene with challenging substrates such as phenol and glycerol show that $Pd(acac)_2$/**1** is a very active catalyst system. The heterogeneous catalyst material can furthermore be easily recovered. High activities and selectivities were obtained under solvent and base-free conditions and in the case of glycerol telomerisation, **1** outperforms its homogeneous analogue PPh_3. Increase of the ligand to metal ratio results in markedly improved product selectivities and reduced metal leaching. Based on these results, it is anticipated that this phosphorus-based COF and related materials can be applied as catalyst supports in a wide variety of metal/phosphine-catalyzed reactions.

Experimental

General remarks

All reactions were carried out under inert atmosphere at room temperature using standard Schlenk techniques. Solvents were dried and distilled under inert atmosphere prior to use. 4,4′-Dibromobiphenyl, phosphorus trichloride, *n*-butyllithium (1.6 M in hexanes), phenol and glycerol were obtained from Acros. Phenyllithium (1.8 M in Et_2O) and palladium acetylacetonate were obtained from Aldrich. Powder XRD data were collected using a Bruker D8 ADVANCE diffractometer with a Co Kα source. Patterns were obtained from 5–70° 2θ using a step size of 0.03° 2θ and a collection time of 1 s per step. TGA was performed on a TGA Q50 Thermographic analyzer from TA Instruments. DSC was performed on a DSC Q2000 from TA Instruments. N_2 adsorption and desorption measurements were performed at liquid nitrogen temperature on a Micromeritics Tristar 3000. Prior to measurement, samples were degassed in nitrogen flow at 90 °C for 14 h. Micropore volumes and mesopore surface areas were determined using *t*-plot analysis using carbon as reference. Solid-state MAS ^{13}C and ^{31}P NMR experiments were performed on a 500 MHz instrument (Bruker Biospin, Germany) using a 4 mm triple resonance ^{1}H, ^{31}P, ^{13}C MAS probehead at 40 °C. ^{31}P spectra were recorded using a 90 degree pulse excitation at a radio-frequency field strength of 50 kHz. ^{13}C data (see also ESI†) were acquired using cross polarization (CP).[28] During acquisition, continuous wave ^{1}H decoupling at 83 kHz was employed. Solid state NMR 1D experiments were recorded with MAS rates of 10 kHz and 12 kHz to identify the spinning sidebands. DRIFT-IR spectra were measured on a TENSOR machine from Bruker. GC analysis was performed on a Shimadzu GC-2010 system with a WCOT fused silica column (25 m × 0.25 mm, CP-WAX 57CB). Elemental analysis was carried out by Kolbe, Microanalytische laboratorium, Mülheim a/d Ruhr, Germany.

Synthesis of 1

To a solution of 4,4′-dibromobiphenyl (6.24 g, 20.0 mmol) in Et_2O (150 mL) was added ^{n}BuLi (50 mL, 80 mmol, 1.6 M in hexanes) and left to stir for 1 h. The resulting pale white suspension was filtered over a glass filter and the isolated solids were suspended in hexane (200 mL). After stirring for 5 min the suspension was filtered over a glass filter and the isolated solids were suspended in THF (120 mL). To this, a solution of PCl_3 (1.79 g, 13.0 mmol) in THF (60 mL) was slowly added dropwise using an addition funnel. Subsequently, phenyllithium (10 mL, 18 mmol, 1.8 M in Et_2O) was added and the dark purple suspension left to react overnight. MeOH (10 mL) was added and left to react for 10 min. The pale suspension was filtered over a glass filter and the isolated solid was suspended in MeOH (200 mL) and stirred for 1 h. These steps were repeated and after filtration the solid was stirred in Et_2O (200 mL). After filtration, the obtained solid was finally dried overnight *in vacuo* at 60 °C. **1** (3.56 g) was obtained as a pale yellow powder. Elemental analysis: found (%): C, 77.20; H, 5.34; O, 5.11; P, 10.08.

Maximum $Pd(acac)_2$ loading per phosphorus

1 (155 mg, 0.50 mmol P) and $Pd(acac)_2$ (211 mg, 0.69 mmol) were stirred in MeOH (60 mL) for 1 hour. The suspension was centrifuged at 2400 rpm for 5 min and the solution decanted. The solids were dried overnight *in vacuo* at 60 °C. 241 mg of $Pd(acac)_2$ loaded catalyst was obtained. Elemental analysis: 0.52Pd@**1**, found (%): C, 62.03; H, 4.85; O, 8.12; P, 7.21; Pd, 12.87.

Heterogeneous catalyst preparation

1 and $Pd(acac)_2$ were mixed in appropriate amounts and stirred overnight in MeOH (20 mL). The solvent was removed *in vacuo* and the obtained solids dried overnight *in vacuo* at 60 °C. Elemental analysis: 1.07Pd@**1**, found (%): C, 55.55; H, 4.66; O, 14.12; P, 5.31; Pd, 19.50; 0.29Pd@**1**, found (%): C, 66.65; H, 4.92; O, 5.11; P, 8.82; Pd, 8.73; 0.15Pd@**1**, found (%): C, 70.93; H, 5.18; O, 9.86; P, 7.52; Pd, 4.00.

50 mL high-pressure glass reactor telomerisation experiments

Phenol telomerisation experiments were conducted in a 50 mL high-pressure glass vessel with Teflon liner and a pressure cap (15 bar) from Salm en Kip. The substrate and catalyst and a magnetic stirring bar were introduced in the glass vessel. The vessel was flushed with N_2 and cooled to −20 °C using a dry ice–acetone bath. A gas inlet tubing (butadiene) was placed in the vessel and the top of the vessel was closed with parafilm. Butadiene was condensed directly in the vessel using a calibrated flow and the total amount of introduced butadiene was determined gravimetrically (err. ±0.1 mg). The reactor was closed and the contents was stirred and heated to 80 °C using an oil bath and heating plate fitted with a thermocouple. After the end of the reaction, the reactor was cooled to −20 °C and opened. The contents were diluted with toluene and transferred to a 100 mL volumetric flask, filtered and analyzed by GC.

100 mL stainless steel autoclave telomerisation experiments

Glycerol telomerisation experiments were conducted in a 100 mL stainless steel autoclave with overhead stirrer from Parr.

The substrate and catalyst were introduced in the autoclave cup and the autoclave was assembled and sealed. The autoclave was flushed two times with 10 bar N_2 or argon and subsequently cooled to −70 °C using a dry ice–acetone bath. Butadiene was condensed directly in the autoclave using a calibrated flow. The total amount of butadiene added was determined gravimetrically (err. ±0.1 g). The contents were heated to 80 °C and stirred vigorously. After the end of the reaction, the reactor was opened to vent the remaining butadiene. The reactor was disassembled and the content was diluted with ethanol and transferred in a 100 mL volumetric flask. 1 mL aliquots were peracetylated in 10 mL Ac_2O/Py (1 : 1 v/v), overnight at room temperature. The resulting solution was diluted with ethanol and transferred to a 50 mL volumetric flask and analyzed by GC.

Acknowledgements

The authors kindly thank Marjan Versluis and Cor van der Spek for the SEM and TEM measurements and ACTS-ASPECT for financial support. MB thanks NWO for financial support (grant 700.26.121).

Notes and references

1 (*a*) P. A. Chase, R. J. M. Klein Gebbink and G. van Koten, *J. Organomet. Chem.*, 2004, **689**, 4016; (*b*) A. Berger, R. J. M. Klein Gebbink and G. van Koten, *Top. Organomet. Chem.*, 2006, **20**, 1.

2 (*a*) J. M. Fraile, J. L. Garcia and J. A. Mayoral, *Chem. Rev.*, 2009, **109**, 360; (*b*) P. Barbaro and F. Liguori, *Chem. Rev.*, 2009, **109**, 515; (*c*) J. Lu and P. H. Toy, *Chem. Rev.*, 2009, **109**, 815.

3 A. Corma, H. Garcia and F. X. Llabres i Xamena, *Chem. Rev.*, 2010, **110**, 4606.

4 Y. Zhang and S. N. Riduan, *Chem. Soc. Rev.*, 2012, **41**, 2083–2094.

5 (*a*) A. M. Bohnsack, I. A. Ibarra, P. W. Hatfield, J. W. Yoon, Y. K. Hwang, J.-S. Chang and S. M. Humphrey, *Chem. Commun.*, 2011, **47**, 4899; (*b*) A. J. Nuñez, L. N. Shear, N. Dahal, I. A. Ibarra, J. W. Yoon, Y. K. Hwang, J.-S. Chang and S. M. Humphrey, *Chem. Commun.*, 2011, **47**, 11855.

6 R. Palkovits, M. Antonietti, P. Kuhn, A. Thomas and F. Schuth, *Angew. Chem., Int. Ed.*, 2009, **48**, 6909.

7 S.-Y. Ding, J. Goa, Q. Wang, Y. Zhang, W.-G. Song, C.-Y. Su and W. Wang, *J. Am. Chem. Soc.*, 2011, **133**, 19816.

8 Q. Zhang, S. Zhang and S. Li, *Macromolecules*, 2012, **45**, 2981.

9 (*a*) S. Bouquillon, J. Muzart, C. Pinel and F. Rataboul, *Top. Curr. Chem.*, 2010, **295**, 93; (*b*) P. C. A. Bruijnincx, R. Jastrzebski, P. J. C. Hausoul, R. J. M. Klein Gebbink and B. M. Weckhuysen, *Top. Organomet. Chem.*, 2012, **39**, 45.

10 R. Palkovits, I. Nieddu, R. J. M. Klein Gebbink and B. M. Weckhuysen, *ChemSusChem*, 2008, **1**, 193.

11 (*a*) J. Briggs, J. Patton, S. Vermaire-Louw, P. Margl, H. Hagen and D. Beigzadeh, WO2010019360 A2, 2009; (*b*) M. J.-L. Tschan, E. J. Garcia-Suarez, Z. Freixa, H. Launay, H. Hagen, J. Benet-Buchholz and P. W. N. M. van Leeuwen, *J. Am. Chem. Soc.*, 2010, **132**, 6463; (*c*) J. R. Briggs, H. Hagen, J. Samir and J. T. Patton, *J. Organomet. Chem.*, 2011, **696**, 1677; (*d*) M. J.-L. Tschan, J.-M. Lopez-Valbuena, Z. Freixa, H. Launay, H. Hagen, J. Benet-Buchholz and P. W. N. M. van Leeuwen, *Organometallics*, 2011, **30**, 792.

12 (*a*) R. Jackstell, S. Harkal, H. Jiao, A. Spannenberg, C. Borgmann, D. Roettger, F. Nierlich, M. Elliot, S. Niven, K. Cavell, O. Navarro, M. S. Viciu, S. P. Nolan and M. Beller, *Chem.–Eur. J.*, 2004, **10**, 3891; (*b*) R. Jackstell, G. A. Andreu, A. Frisch, K. Selvakumar, A. Zapf, H. Klein, A. Spannenberg, D. Rottger, O. Briel, R. Karch and M. Beller, *Angew. Chem., Int. Ed.*, 2002, **41**, 986.

13 (*a*) C. U. Pittman Jr., S. U. Wuu and S. E. Jacobson, *J. Catal.*, 1976, **44**, 87; (*b*) K. Kaneda, H. Kurosaki, M. Terasawa, T. Imanaka and S. Teranishi, *J. Org. Chem.*, 1981, **46**, 2356; (*c*) F. Benvenuti, C. Carlini, A. M. R. Galleti, G. Sbrana, M. Marchionna and R. Patrini, *J. Mol. Catal. A: Chem.*, 1999, **137**, 49; (*d*) F. Benvenuti, C. Carlini, M. Marchionna, R. Partini, A. M. R. Galleti and G. Sbrana, *J. Mol. Catal. A: Chem.*, 1999, **139**, 177.

14 (*a*) B. I. Lee, K. H. Lee and J. S. Lee, *J. Mol. Catal. A: Chem.*, 2000, **156**, 283; (*b*) J. M. Lopes, Z. Petrovski, R. Bogel-Lukasik and E. Bogel-Lukasik, *Green Chem.*, 2011, **13**, 2013; (*c*) L. Conceicao, R. Bogel-Lukasik and E. Bogel-Lukasik, *Green Chem.*, 2012, **14**, 673.

15 A. Behr, M. Becker, T. Beckmann, L. Johnen, J. Leschinski and S. Reyer, *Angew. Chem., Int. Ed.*, 2009, **48**, 3598.

16 A. N. Parvulescu, P. J. C. Hausoul, P. C. A. Bruijnincx, S. T. Korhonen, C. Theodorescu, R. J. M. Klein Gebbink and B. M. Weckhuysen, *ACS Catal.*, 2011, **1**, 526.

17 (*a*) M. Rose, W. Böhlmann, M. Sabo and S. Kaskel, *Chem. Commun.*, 2008, 2462; (*b*) J. Fritsch, M. Rose, P. Wollmann, W. Böhlmann and S. Kaskel, *Materials*, 2010, **3**, 2447; (*c*) J. Fritsch, F. Drache, G. Nickerl, W. Böhlmann and S. Kaskel, *Microporous Mesoporous Mater.*, 2013, **172**, 167.

18 M. Wander, P. J. C. Hausoul, L. A. J. M. Sliedrecht, B. J. van Steen, G. van Koten and R. J. M. Klein Gebbink, *Organometallics*, 2009, **28**, 4406.

19 M. A. Perez, E. Longo and C. A. Taft, *THEOCHEM*, 2000, **507**, 97.

20 M. Baldus, *Prog. Nucl. Magn. Reson. Spectrosc.*, 2002, **41**, 1–47.

21 (*a*) F. Micoli, L. Salvi, A. Salvini, P. Frediani and C. Gianelli, *J. Organomet. Chem.*, 2005, **690**, 4867; (*b*) M. Joshaghani, E. Faramarzi, E. Rafiee, M. Daryanavard, J. Xiao and C. Baillie, *J. Mol. Catal. A: Chem.*, 2006, **259**, 35.

22 R. A. Komorski, A. J. Magistro and P. P. Nicholas, *Inorg. Chem.*, 1986, **25**, 3917–3925.

23 (*a*) S. Baba, T. Ogura and S. Kawaguchi, *Bull. Chem. Soc. Jpn.*, 1974, **47**, 665; (*b*) L. B. Belykh, T. V. Goremyka, N. I. Skripov, V. A. Umanets and F. K. Schmidt, *Kinet. Catal.*, 2006, **47**, 367; (*c*) V. S. Tkach, D. S. Suslov, N. V. Kurat'eva, M. V. Bykov and M. V. Belova, *Russ. J. Coord. Chem.*, 2011, **37**, 752.

24 V. S. Tkach, D. S. Suslov, G. Myagmarsuren, G. V. Ratovskii, A. V. Rohin, T. Felix and F. K. Schmidt, *J. Organomet. Chem.*, 2008, **693**, 2069.

25 (*a*) F. Vollmüller, J. Krause, S. Klein, W. Mägerlein and M. Beller, *Eur. J. Inorg. Chem.*, 2000, 1825; (*b*) P. J. C. Hausoul, S. D. Tefera, J. Blekxtoon, P. C. A. Bruijnincx, R. J. M. Klein Gebbink and B. M. Weckhuysen, *Catal. Sci. Technol.*, 2013, **3**, 1215, DOI: 10.1039/c2cy20522j.
26 C. Goux, M. Massacret, P. Lhoste and D. Sinou, *Organometallics*, 1995, **14**, 4585.
27 (*a*) P. W. Jolly and N. Kokel, *Synthesis*, 1990, 771; (*b*) A. Döhring, R. Goddard, G. Hopp, P. W. Jolly, N. Kokel and C. Krüger, *Inorg. Chim. Acta*, 1994, **222**, 179; (*c*) E. Kuntz, J.-M. Basset, D. Bouchu, G. Godard, F. Lefebvre, N. Legagneux, C. Lucas and D. Michelet, *Organometallics*, 2010, **29**, 523.
28 A. Pines, M. G. Gibby and J. S. Waugh, *J. Chem. Phys.*, 1973, **59**, 569–590.